Electronic Structure Pseudopotential Calculations of Large (.apprx.1000 Atoms) Si Quantum Dots

ARTICLE *in* THE JOURNAL OF PHYSICAL CHEMISTRY · FEBRUARY 1994

Impact Factor: 2.78 · DOI: 10.1021/j100059a032

2 AUTHORS:

Lin-Wang Wang
Lawrence Berkeley National Laboratory
336 PUBLICATIONS **10,999** CITATIONS
SEE PROFILE

Alex Zunger
University of Colorado Boulder
768 PUBLICATIONS **51,120** CITATIONS
SEE PROFILE

Electronic Structure Pseudopotential Calculations of Large (~1000 Atoms) Si Quantum Dots

Lin-Wang Wang and Alex Zunger*

National Renewable Energy Laboratory, Golden, Colorado 80401

*Received: September 30, 1993; In Final Form: December 15, 1993**

The electronic structure of quantum dots containing $N \geq 1000$ atoms is difficult to calculate by conventional molecular methods since the effort scales as N^3. Our newly developed method allows calculation of eigenstates within a desired "energy window" and thus has a linear-in-N scaling. This method is applied here to Si quantum dots using a plane wave basis expansion and an empirical pseudopotential Hamiltonian. Hydrogen atoms passivate the surface dangling bonds using a realistic surface relaxation geometry. We investigate the dependences of energy gaps and radiative recombination rates on the size, shape, and orientation of the Si quantum dots. We find that (1) a unified curve exists for band gap *vs* size of quantum spheres, cubes, and rectangular boxes; (2) the band edge states of Si quantum dots are bulklike, not surfacelike; (3) the band gap is insensitive to the surface orientation and to the overall shape of the quantum dot as long as it is not too prolate; (4) the radiative lifetime is sensitive to the shape and orientation; and (5) effective mass and single band truncated crystal models describe inadequately the electronic structure of Si quantum dots in the size range (≲40 Å) studied here.

I. Introduction: The Basic Problem and Theoretical Strategies

Quantum confinement at reduced dimensions leads to fascinating changes in the optical properties relative to those of the 3D bulk materials.[1] Small gap semiconductors are particularly interesting in this respect as these black substances can be transformed via control of the shape and size of the quantum structure into materials whose color can extend throughout the visible range.[2] Nanometer size silicon particles are an example of semiconductor quantum structure, which have been made by vaporization of Si electrodes,[3] microwave plasma decomposition of SiH_4,[4] and gas-phase pyrolysis of disilene.[5] A related development in the area of Si nanostructure is the discovery of intense, blue-shifted photoluminescence from "porous Si".[6] One explanation for this blue shift[7] is that the microstructure consists of islands of isolated quantum dots, each experiencing quantum confinement. These experimental developments in the area of silicon nanostructures have raised a number of questions which we will attempt to address in this work:

(i) Given the relatively large surface-to-volume ratio in small quantum dots, one wonders to what extent are their optical properties decided by surface phenomena (reconstruction, chemisorption) as opposed to bulk-intrinsic quantum size effects. In particular, are the band edge wave functions "bulklike" or "surfacelike"?

(ii) In its simplest form, the notion of quantum confinement addresses the "smallness" effects, without reference to the shape of the small objects. However, current quantum dot formation methods are likely to produce not only a distribution of sizes but also a distribution of "isomers" (various shapes and surface orientations) for each size. One then needs to know what is the dependence of the band gap on the shape of the quantum dot (sphere, box, rectangular, etc.) or the orientation of its surface planes [e.g., (001) *vs* (110)].

(iii) While the effects of size on transition energies (band gap) are rather well studied, the effects of size and shape on transition probabilities (radiative recombination rate) are known to a lesser extent.

Addressing these issues requires an electronic structure theory. While ultrasmall quantum dots (≤100 atoms) can be treated by molecular methods such as the *ab-initio* Hartree–Fock[8] or local density approximation (LDA),[9] considerable experimental interest exists in larger quantum dots (≥1000 atoms) for which such methods appear impractical. Three classes of electronic structure approaches exist for such large sizes:

(*i*) *The Effective Mass Approximation (EMA).*[10] Here one replaces the microscopic quasi-periodic potential $V(\mathbf{r})$ (which exists inside the material) by a constant potential, while the kinetic energy operator is replaced by an effective mass operator, derived from the parabolic expansion of the bulk band structure. The EMA treats "large systems" accurately and can be extended to incorporate multiband coupling ("band mixing").[11] However, for the sizes studied here (≤40 Å), the parabolic band approximation might not be valid. This will be tested below.

(*ii*) *The Truncated Crystal Method (TC).*[12,13] Instead of using parabolic bands, this method uses the actual dispersion relation of the bulk band structure and approximates the quantum dot wave functions by a sum of a few bulk Bloch wave functions of a single band at different wavevectors. It ignores band mixing and can be applied only to simple quantum dot geometries. It has been tested by comparison with direct calculations for 2D films[13a] and works very well. However, the formula of Rama Krishna and Friesner[12] for 0D quantum dots remains untested relative to direct calculations. This will be tested below.

(*iii*) *Direct Molecular Calculations.* In this approach one diagonalizes the microscopic Hamiltonian consisting of the full kinetic energy and quasi-periodic atomic potential, thus avoiding the approximations of methods i and ii. However, because full variational *ab-initio* approaches to this Hamiltonian are impractical, the Hamiltonian or its basis representations are usually simplified. In the widely used tight binding (TB) model[14] a small, implicit basis set (4–5 orbital per atom) is used; the function form of the basis function is, however, undermined, since only the empirically adjusted Hamiltonian matrix elements are used. The small basis suggests limited variational flexibility, particularly for the conduction bands. Furthermore, because the lack of explicit basis functions, it is difficult to correctly describe the dependence of the Hamiltonian matrix elements on the atomic geometry (e.g., on the surface structure of the quantum dot) or to compare the $\vec{r}$-space wave functions $\psi(\vec{r})$ with the results of *ab-initio* calculations on smaller reference systems. Another version is the linear combination of atomic orbitals (LCAO)[15] method in which explicit basis functions are used. This method is usually applied to rather small quantum dots (≤100 atoms) while applications to larger systems require a drastic truncation of the basis set size.

* Abstract published in *Advance ACS Abstracts,* February 1, 1994.

0022-3654/94/2098-2158$04.50/0

Most of these difficulties can be overcome by the empirical pseudopotential method (EPM)[16] which we will use here. The EPM approximates the total screened potential $V(\mathbf{r})$ in $\hat{H} = -^1/_2\nabla^2 + V(\mathbf{r})$ by a superposition of atomic pseudopotentials $V_{atom}(|\mathbf{r}|)$, i.e.

$$V(\mathbf{r}) = \sum_{R_{atom}} V_{atom}(|\mathbf{r} - \mathbf{R}_{atom}|) \quad (1)$$

where the "effective potential" $V_{atom}(|\mathbf{r}|)$ is adjusted to fit either experimental or *ab-initio* calculated data on relevant prototype systems. In the present work we have fitted V_{atom} to the bulk Si band structure, effective masses, and the surface work function. The quantum dot wave functions are expanded in a large basis of plane waves:

$$\psi_j(\mathbf{r}) = \sum_{\mathbf{G}} B_j(\mathbf{G}) e^{i\mathbf{G}\mathbf{r}} \quad (2)$$

where G is a reciprocal vector and $B_j(\mathbf{G})$ are the expansion coefficients to be determined variationally. Although the basis set (2) is not atomiclike, it can be increased systematically, and the product $\hat{H}\psi$ can be evaluated both accurately and easily.[17] The atomic structure $\{\mathbf{R}_{atom}\}$, including realistic surface relaxations, is taken from experiment and/or *ab-initio* total energy calculations on prototype systems.

The remaining problem is to solve the single-particle Schrodinger's equation:

$$\hat{H}\psi_j = \epsilon_j\psi_j \quad (3)$$

for a ~1000-atom quantum dot given the representations of eqs 1 and 2. Conventional variational methods[17] force one to calculate all occupied eigensolutions even though one is interested here only in the HOMO and LUMO. Thus, if a variationally accurate basis set is used, conventional methods for solving eq 3 are generally limited to ≤100-atom systems. We have developed a new method[18] which permits calculating the energy eigenstates within an "energy window", so the effort scales linearly with the system's size. It can thus be used with modest computational effort to solve ~1000-atom systems with a variationally accurate basis set. We will use here this new method along with our recently developed Si and H empirical pseudopotentials (see below) to study the questions raised in this section.

In summary, we will use a direct calculation approach to the electronic structure of Si quantum dots, obviating the effective mass approximation. We include nonparabolic bands, interband coupling, realistic surface relaxations, and a large basis set. The main approximations are the use of a local and non-self-consistent pseudopotential. We will study the dependence of the band gap of Si quantum dots on (i) size, (ii) shape, and (iii) surface orientation and compare our results to previous model calculations (the EMA[10] and the TC[12]), direct calculations, and experiments.[3-5]

II. Details of Calculation

A. The Si and H Pseudopotentials and the Surface Relaxation Model. The application of the empirical pseudopotential method to band structure and optical spectra of extended solids is reviewed in ref 16. In the classic EPM, the pseudopotential $V(\vec{G})$ is defined only on the discrete bulk reciprocal lattice vectors $\{\vec{G}_i\}$. To describe a finite quantum dot, one needs a continuous momentum space form $V_{Si}(q)$, so the original bulk EPM's are insufficient. We have fitted the local pseudopotential of the form[13a]

$$V_{Si}(q) = a_1(q^2 - a_2)/(a_3e^{a_4q^2} - 1) \quad (4)$$

to the bulk band structure, effective masses, and the work function.[19-26] This gave $a_1 = 0.2685$, $a_2 = 2.19$, $a_3 = 2.06$, and $a_4 = 0.487$ in atomic units (hartrees for energy, bohr^{-1} for momentum q). Table 1[19-26] compares these quantities as obtained with the current EPM, the bulk EPM of Chelikowsky and Cohen,[27] and experiment. It is clear from Table 1 that the two empirical pseudopotentials have similar quality; the band energies are within 0.1 eV of the experimental data (i.e., similar to the experimental uncertainty). Figure 1 compares the current atomic Si pseudopotential $V_{Si}(q)$ with the screened LDA potential, showing that the two are very close. Thus, one can think of our empirical pseudopotential as a modification of the LDA potential such that the resulting band structure (especially the band gap) is corrected. This is the main advantage of our empirical pseudopotential method over tght-binding-like methods.

Surface passivation of the Si quantum dots[3-5] was modeled by saturating all dangling bonds with hydrogen atoms. The surface of a quantum dot can usually be represented as a combination of "patches" of the primary (111), (110), and (100) surfaces of Si films. [If it is not, a few atoms are added or removed from the surface to make it so.] This correction is minor, so the overall

TABLE 1: Comparison of the Si Bulk Band Structures and Effective Masses, As Obtained in the Present EPM (Eq 4) and in the Bulk EPM of Chelikowsky and Cohen,[27] Respectively[a]

property	present EPM	bulk EPM (ref 27)	experiment
$\Gamma_{25'v}$	0	0	0
Γ_{1v}	-12.57	-12.68	-12.5(6)[f]
Γ_{15c}	3.24	3.34	3.35(1)[b]
$\Gamma_{2'c}$	4.12	4.19	4.15(5)[c]
$L_{2'v}$	-10.19	-10.26	-9.3(4)[f]
L_{1v}	-7.25	-7.33	-6.8(2)[f]
$L_{3'v}$	-1.28	-1.27	-1.2(2)[c]
L_{1c}	2.18	2.13	2.04(6)[d]
L_{3c}	4.02	3.88	3.9(1)[c]
X_{4v}	-3.01	-3.03	-2.9[e]
X_{1c}	1.32	1.14	1.13(?)[b]
Σ_{min}	-4.47	-4.55	-4.48[c]
E_{gap}	1.167	1.062	1.124[g]
W	4.96		4.9[i]
$m_L(e)$	0.928	0.912	0.916[g]
$m_T(e)$	0.199	0.194	0.19[g]
$m^{(2)}_{\Gamma-X}(h)$	0.272	0.271	0.34[h]
$m^{(1)}_{\Gamma-X}(h)$	0.168	0.170	0.15[h]
$m^{(2)}_{\Gamma-L}(h)$	0.669	0.676	0.69[h]
$m^{(1)}_{\Gamma-L}(h)$	0.098	0.097	0.11[h]

[a] We use a cutoff energy of 4.5 Ry for the plane wave expansion and a Si bulk lattice constant of 5.43 Å. The last column gives experimental values. The numbers in parentheses of the experimental data indicate the estimated error in the last digit. $m^{(i)}_{\Gamma-X}(h)$ and $m^{(i)}_{\Gamma-L}(h)$ stand for the non-spin-coupled effective hole mass on the Γ–X and Γ–L directions (defined as $(\hbar k)^2/2\Delta E$); i denotes the degeneracy of the band. W is the work function. Energies are in eV, and effective masses are in the unit of electron mass. [b] From ref 19. [c] From ref 20. [d] From ref 21. [e] From ref 22. [f] From ref 23. [g] From ref 24. [h] From ref 25. [i] From ref 26.

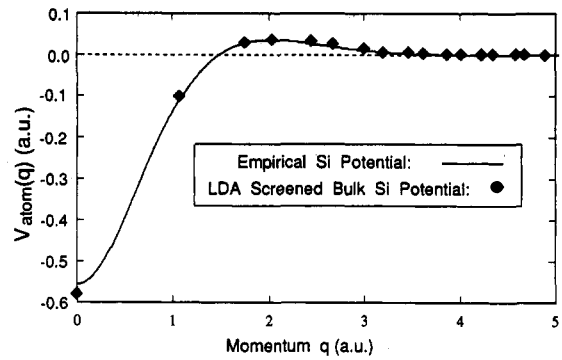

Figure 1. Comparison between the present empirical Si pseudopotential and a first-principles screened local pseudopotential obtained in self-consistent LDA calculation. The total LDA screened potential is decomposed into atomic potentials according to $\sum_R e^{iR_iG}V_{atom}(G) = V(G)$, where G is the bulk reciprocal lattice vector and R_i is the Si atomic positon.

shape of the quantum dot does not change. The precise relaxation of the quantum dot surface atoms is taken from data on these three primary surfaces of H-covered Si films. The reconstructed surface geometries we used are (1×1):H for the (111)-oriented film surface,[28,29] (1×1):H for the (110)-oriented film surface,[30] and (1×1):2H for the (100)-oriented film surface.[31,32] The previously determined relaxations for (111) and (110) surfaces are relatively small,[33] so for these surfaces we used an ideal unrelaxed structure with Si–H bond distance of 1.487 Å. There are different relaxation models[34] for the (100) (1×1):2H surface. We have used a "canted dihydride" model of Northrup,[34] derived from a LDA total energy minimization.

The hydrogen pseudopotential was obtained by fitting the surface local density of states of our primary surfaces to the data of ultraviolet photoemission spectroscopy (UPS)[29,30] and angle-resolved electron-energy-loss spectroscopy (AR-EELS).[31] The antibonding conduction band surface states was fitted to the LDA result placing these states at ≥1 eV above the conduction band minimum.[35] Fitting all these data results in the following H empirical pseudopotential in atomic units:

$$V_H(q) = -0.1416 + 9.802 \times 10^{-3} q + 6.231 \times 10^{-2} q^2 - 1.895 \times 10^{-2} q^3; \quad \text{when } q \le 2$$

$$V_H(q) = 2.898 \times 10^{-2}/q - 0.3877/q^2 + 0.9692/q^3 - 1.022/q^4; \quad \text{when } q > 2 \quad (5)$$

B. Solving Schrodinger's Equation in a Linear-in-Size Fashion. Having determined the pseudopotentials and surface relaxation model, we can now construct the product $\hat{H}\psi = [-{}^1/_2\nabla^2 + V(\mathbf{r})]\cdot\psi(\mathbf{r})$. Using the conventional variational minimization methods based on eq 3, one is forced to calculate all occupied eigenstates starting from the lowest one. Such methods lead to a N^3 scaling,[17] where N is the number of atoms in the system. This makes the conventional method impractical, unless the basis set is heavily truncated, as in the tight-binding method. However, here we are interested only in the highest occupied and in the lowest unoccupied states. A central point is that the eigensolutions ψ_j of eq 3 also satisfy

$$(\hat{H} - \epsilon_{ref})^2\psi_j = (\epsilon_j - \epsilon_{ref})^2\psi_j \quad (6)$$

where ϵ_{ref} is a reference energy placed inside the band gap. Thus, instead of minimizing $E = \int\psi_j(r)\,\hat{H}\psi_j(r)\,d^3r$ and computing thousands of $\psi_j(r)$'s, like in the conventional method,[17] we minimize the quantity

$$F = \int\psi_j(r)(\hat{H} - \epsilon_{ref})^2\psi_j(r)\,d^3r \quad (7)$$

for just a few $\psi_j(r)$'s. The state with the lowest F is the eigenstate of $\hat{H}$ with eigenvalue ϵ_j closest to ϵ_{ref}. Thus, this state is either the highest occupied molecular orbital (HOMO) or the lowest unoccupied molecular orbital (LUMO). The initial guess of ϵ_{ref} is obtained by performing a single conventional calculation (eq 3) on a small cluster. Shifting ϵ_{ref} inside the band gap will ensure that both the HOMO and the LUMO are captured by this method. The function F is minimized with respect to the plane wave coefficients $B_j(G)$ using a carefully preconditioned conjugate gradient scheme.[18] Using this scheme, the solution for the $Si_{1315}H_{460}$ quantum dot takes 2 h of Cray-YMP CPU time. (We calculated four wave functions on each side of the band gap.) Extrapolating the actual calculation times for small quantum dots, one can show that conventional variational method (i.e., eq 3 rather than eq 6) would take several weeks of continuous Cray-YMP CPU time for the $Si_{1315}H_{460}$ system. Use of our method enables, for the first time, pseudopotential calculations of $O(10^3)$ atom systems. In our calculations, the wave function $\psi_j(\mathbf{r})$ is expanded as in eq 2. The cutoff energy of G in eq 2 is 4.5 Ry,

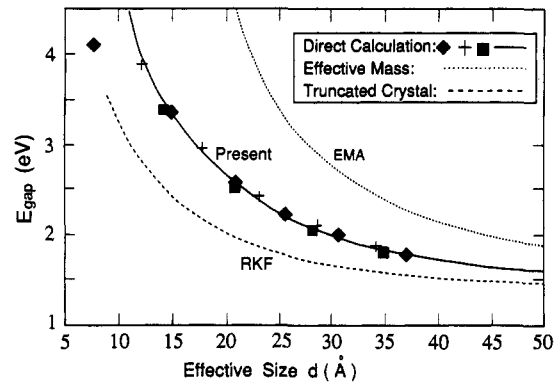

Figure 2. LUMO–HOMO band gap versus the effective sizes $d = (3/4\pi\rho)^{1/3}N_{Si}^{1/3}$ (Å) for the three prototype quantum dot shapes. The symbols ◆, +, and ■ stand for spheres, (110) × (1$\bar{1}$0) × (001) rectangular boxes, and (100) × (010) × (001) cubic boxes, respectively. The fitted solid line is $E_g(d) = 1.1673 + 88.34(d/\text{Å})^{-1.37}$ (eV). Also shown are the multiband effective mass result (EMA)[39] and the result of the method of Rama Krishna and Friesner (RKF)[12] (applied here to cubic quantum dots with the present Si pseudopotential of eq 4). In all cases, the excitonic Coulomb shift (eq 9) is excluded.

and the same cutoff is used in the fitting of above $V_{Si}(q)$ and $V_H(q)$. The transformation between $\psi_j(r)$ on a real space grid and $B_j(G)$ on a reciprocal space grid is done by numerical fast Fourier transform (FFT).[36] For the largest quantum dot considered here, there are 1315 Si atoms, 460 H atoms, and 100 × 100 × 100 real space FFT grid points. Further detail of this method will be described elsewhere.[18]

III. Results

A. Dependence of the Band Gap on Size for Si Spheres, Cubes, and Rectangular Boxes. The most commonly addressed question in quantum dot physics is the size dependence of the energy gap.[1] However, experimentally prepared quantum dots not only have different sizes, but for each size there could be a distribution of shapes and surface orientations. Although in some cases the synthesized particles[3-5] are assumed to have a spherical shape, a variety of quantum dot shapes were proposed[37] in the porous silicon materials. To understand the effects of the shapes on the energy levels of quantum dots, we study here three "primary prototype shapes": (i) spherical balls, (ii) rectangular boxes [the surfaces are in the (110), (1$\bar{1}$0), and (001) directions and the lengths of the edges satisfy $L_x = L_y = L_z/\sqrt{2}$], and (iii) cubic boxes [the surfaces are in the (001), (010), and (100) directions]. To compare the electronic properties of these different prototype shapes, we need a consistent definition of the quantum dot's size. A natural choice is to associate the effective size with the diameter of a sphere which has the mass density ρ of bulk Si and contains the same number N of silicon atoms as the quantum dot in question. Then, $d(N) = (3/4\pi\rho)^{1/3}N^{1/3} = 3.3685N^{1/3}$ (Å). Using this definition, the calculated size dependence of the LUMO–HOMO band gaps of the three prototype quantum dots is depicted as symbols and the solid line in Figure 2. Quite surprisingly, the three sets of data corresponding to the three prototype quantum dots collapse into a single unified curve. Thus, if we measure the effective size by $d \propto N^{1/3}$ and vary N, the gaps of all prototype shapes (which are not too prolate) fall on a "universal" curve.

B. Quantum Dot Wave Functions and the Role of Surface Atoms. Having presented the global variation of the energy gaps, we next describe the basic characteristics of the wave functions. Shown in Figure 3a,b are the wave function square of the LUMO and HOMO of the rectangular quantum box with $d = 34.1$ Å ($N_{Si} = 1035$). While other quantum dots represented in Figure 2 may have different wave function patterns, in all cases, the HOMO and LUMO states are found to be localized in the interior of the quantum dot with zero amplitude on the surfaces. Because of this and the fact that hydrogen potential is of very short range, we find that the surface hydrogen atoms play little direct role in

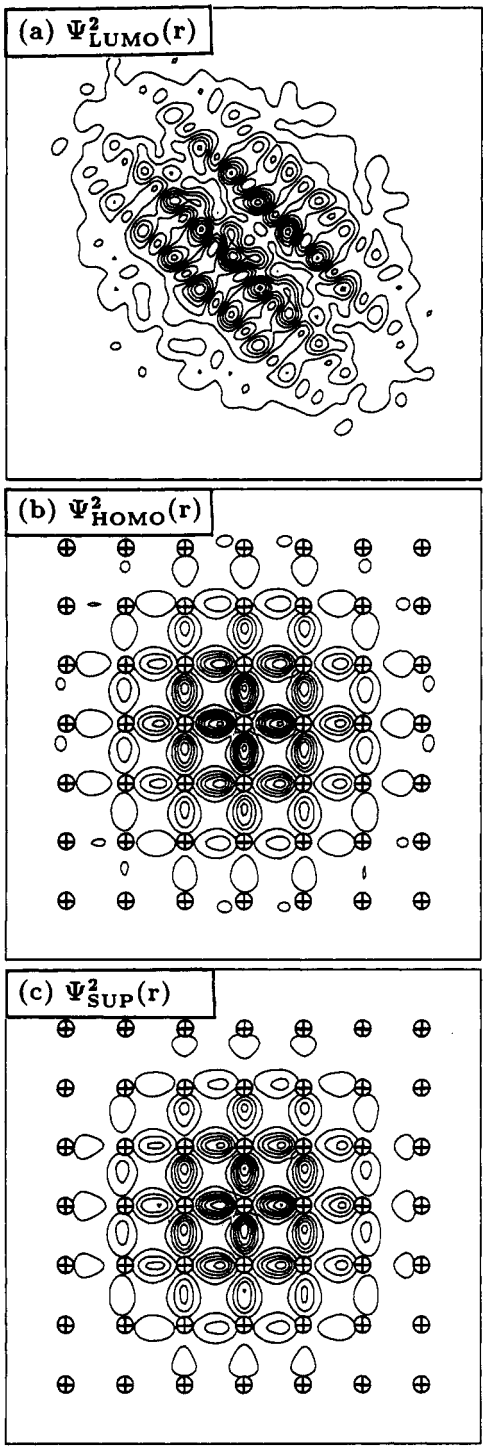

Figure 3. Wave function square contour plots of the (110) × (1$\bar{1}$0) × (001) rectangular quantum box with d = 34.1 Å and N_{Si} = 1035 viewed from the [001] direction. (a) The LUMO wave function square summed along the z direction. (b) The HOMO wave function square plotted on the $z = L_z/2$ cross section. The crossed circles in (b) and (c) denote the positions of the silicon atoms on that plane. (c) The square of the HOMO wave function reconstructed from eq 8 using just three bulk bands at k^* (see text). This is plotted on the same cross section and has the same contour steps as in (b).

the determination of the wave functions and hence the band gaps and oscillator strengths. This is in direct conflict with the tight-binding result of Gavrilenko et al.[38] which produces surfacelike features in their LUMO states. In ref 38, the same type of hydride termination on the Si (001) surface is used as in the present work, but the surface atomic relaxation is done by total energy calculations based on the tight-binding Hamiltonian. However, we believe that the main reason of the difference is due to the different treatments of the surface H potentials: In ref 38, the energy levels of the SiH_4 molecule are fitted to give the matrix elements of the TB Hamiltonian. We have tested this procedure using EPM and find a similar surfacelike LUMO state. However, we feel that a SiH_4 molecule is not an adequate model for H-covered Si surfaces. On the (001) film surface, there are two H atoms from neighboring H:Si:H groups which can be quite close, but this situation is totally absent in the SiH_4 molecule. Thus, we fit our H potential directly to the local density of state of these surfaces. This shows that the LUMO and HOMO of quantum dots are both bulklike.

Both the effective mass and the truncated crystal methods model the states of quantum structure in terms of an expansion in periodic crystal solutions. It is thus interesting to analyze our directly calculated "exact" wave functions also in terms of bulk Bloch wave functions. We can expand the directly calculated quantum dot state as a linear combination of the bulk Bloch states:

$$\psi_i^{dot} = \sum_{n,k} \alpha_{n,k}^{(i)} \psi_{n,k}^{bulk} \tag{8}$$

where k and n are the wave vector and the band index of the bulk Bloch wave function $\psi_{n,k}^{bulk}$. Consider as an example the rectangular quantum box whose directly calculated wave functions are shown in Figure 3a,b. In a rectangular box, k of eq 8 is quantized as $\pi[\pm j_x L_x^{-1}, \pm j_y L_y^{-1}, \pm j_z L_z^{-1}]$, where j_x, j_y, and j_z are positive integers larger than zero. In a particle-in-a-box model, the lowest energy is obtained for $j_x = j_y = j_z = 1$, denoted here as k^*. We refere to these as the "particle in a box k points". These k^* lie on lines connecting the Γ point with a point between L and K in the first bulk Brillouin zone. We have calculated the projection $P_n = \sum_{k^*} |a_{n,k^*}|^2$ for the quantum dot HOMO state and found that as much as 93% of the amplitude of $|\psi^{dot}_{HOMO}|^2$ comes from the three upper valence bands n_1, n_2, and n_3 at k^*. (These three bands become triply degenerate at the $\Gamma_{25,v}$ point. The remaining 7% comes primarily from other k points for the same bands.) Similar percentage is found in other quantum dots. The projection weights P_{n_1,n_2,n_3} for these three bands are 0.774, 0.005, and 0.149. (The small P_{n_2} value in this case is accidental; for most other cases we tested, these three numbers are comparable.) Figure 3c shows the approximate $\psi^2_{HOMO}(r)$, using just these three bands at k^* in eq 8. We see that this approximation is very close to the directly calculated wave function shown in Figure 3b.

From our analysis of the wave functions, we conclude that (i) the band-edge quantum dot wave functions are "bulklike" in that they can be constructed from just a few bulk Bloch wave functions; (ii) it is essential to have in eq 8 a band mixing since no single bulk band represents accurately the wave function of the quantum dot; and (iii) the k-point selection rules of particle-in-a-box are a reasonable approximation to the exact results.

C. Comparison with Previous Model Calculations. Figure 2 also compares the results of two model calculations with out direct "exact" calculations. These models includes the multiband effective mass approximation[39] and the model of Rama Krishna and Friesner (RKF),[12] recalculated here (for consistency of comparison with the direct calculation results) for cubic boxes using the present pseudopotential. The present pseudopotential and the one used by RKF differ in bulk by less than 0.1 eV.

We start with a comparison of our direct results with the EMA. As we saw above, the HOMO and LUMO states found in our direct calculations are not surface states; hence, a comparison with the results of the (surfaceless) EMA is warranted. Fitting our "exact" calculation gives (solid line of Figure 2) a $E_g(d) = 1.167 + 88.34(d/\text{Å})^{-1.37}$ (eV) scaling, while the effective mass model with an infinite confining wall (shown in Figure 2) predicts a $1/d^2$ scaling. The EMA model overestimates considerably the increase of band gap $[\Delta E_g(d) = E_g(d) - E_g^{bulk}]$ with reduced size, despite the fact that multiband coupling is correctly included in

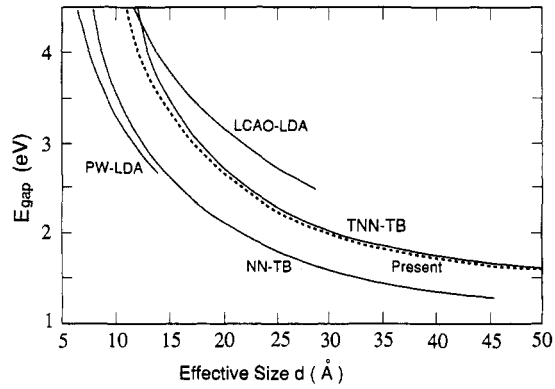

Figure 4. Comparison of calculated LUMO–HOMO gaps *vs* size as obtained with different direct calculation methods. The curve representing the current result is fitted from Figure 2. The results are for PW-LDA,[43] NN-TB,[40] TNN-TB,[41] and LCAO-LDA.[42] See text for definitions of these methods.

this EMA calculation. Replacing in the EMA calculation the infinite confining wall by a finite barrier reduces $\Delta E_g(d)$ and softens the $1/d^2$ scaling. Indeed, solving the EMA equation for a finite barrier of height 4 eV and using an effective mass $m^* = 0.2m$ gives a 10% lower $\Delta E_g(d)$ for $d = 40$ Å and a 15% lower $\Delta E_g(d)$ for $d = 25$ Å. This reduces the EMA error relative to our direct calculations by 20% and 30% for $d = 40$ and 25 Å, respectively. The remaining, bigger part of the error must come from the EMA Hamiltonian itself, i.e., from the assumption of parabolic dispersion.

We next compare our direct results with the model of RKF.[12] The method of RKF, which corrects the parabolic scaling of the effective mass model by explicitly using the dispersion relations of the bulk band structure, underestimates the band gap opening $\Delta E(d)$. For $d = 15$ Å, the RKF method error is ~1 eV out of ~2 eV. The reason for this is the neglect of band mixing: eq 8 suggests that $\epsilon^{dot}_{HOMO} \cong \sum_n P_n \epsilon^{bulk}_n(k^*)/\sum_n P_n$. The simple truncated crystal method uses the same particle-in-a-box k^* value as in the above analysis, computes the bulk bands from a similar empirical pseudopotential, but assumes *ad-hoc* that a single band (the highest) can be used in the sum of eq 8. The neglect of the other lighter bands results therefore in a HOMO that is too high and thus in a band gap that is too small. In the rectangular box example of the previous section, $\epsilon^{bulk}_n(k^*) = (-0.205, -0.555, -1.089)$ eV (measured from the top of bulk valence band) for n_1, n_2, n_3, respectively. Using all three bands gives $\epsilon^{dot}_{HOMO} = -0.348$ eV, which compares well with the directly calculated result –0.338 eV, while using only n_1 gives $\epsilon^{dot}_{HOMO} = -0.205$ eV. Since the single-band TC wave function (eq 8) can satisfy the film boundary condition, it works much better for quantum films[13a] than for quantum wires[13b] or quantum dots.

We conclude from Figure 2 that, at present, there is no simple, shortcut model which can treat correctly both the band mixing and noparabolic band structure dispersion relation in quantum dots. Before such a model becomes available, one has to rely on direct computations to study the properties of quantum dots in the size range considered here.

D. Comparison with Previous Direct Calculations. Figure 4 compares our results for E_g *vs* d with four previous direct calculations: the empirically fitted nearest-neighbor tight-binding (NN-TB) of Ren and Dow,[40] the empirically fitted third-neighbor (nonorthogonal) tight-binding (TNN-TB) model of Proot, Delerue, and Allan,[41] and two LDA calculations—one which uses a small LCAO basis (LCAO-LDA) by Delly and Steigmeier[42] and one which uses a plane wave basis (PW-LDA) by Hirao, Udo, and Murayama[43] but is limited to small ($N_{Si} \leq 123$) quantum dots. In all calculations, an ideal atomic structure (no surface reconstructions and relaxations) was assumed.

We conclude the following: (i) The PW-LDA calculation underestimates the band gap since the intrinsic LDA band gap

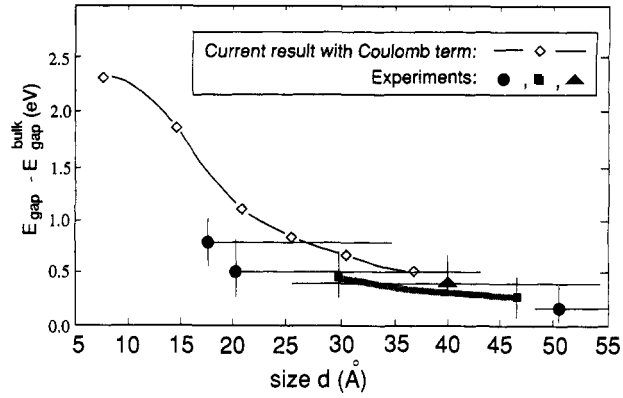

Figure 5. Excitonic gap (eq 9) compared with PL data for spherical quantum dots. The Coulomb interaction is included in the calculated band gap according to eq 9. The symbols ●, ▲, and ■ denote PL data from ref 5, 3, and 4, respectively. The vertical lines represent the widths at half-maximum of the PL spectra. The horizontal lines denote the size distributions. The size distribution for ○ is estimated mostly from TEM and X-ray data in ref 5. The experiment of ref 4 does not report the size distribution. The shaded area represents a range of the experimental points of ref 4. The solid line connecting ◇ represents our calculation.

error[44] was not corrected. (ii) The two TB models differ essentially by a constant shift. Our results agree closely with the TNN-TB, implying that longer than nearest-neighbor interactions (and basis set overlap effects) are important. (iii) The small basis LCAO-LDA results appear to be inaccurate.

E. Comparison of Band Gaps with Experiment. Having found that using our definition of effective size $d(N)$, all prototype shapes give similar band gaps; we can now compare the calculated band gaps with experiment. We will discuss experiments[3-5] which measure the band gap of nearly spherical Si quantum dots by photoluminescence (PL) spectra. The size distribution is measured by high-pressure liquid chromatograph (HPLC), transmission electron microscopic (TEM), and X-ray peak width. The results are summarized in Figure 5. There, we use a solid symbol to represent each sample and a crossing horizontal line to indicate the width of the size distribution for that sample. For the data from ref 5, we put the symbol at the X-ray position and mostly ignore the HPLC value because it tends to overestimate the size due to the aggregation of monomers. As can be seen, there is a very wide size distribution in these particles. A vertical line passing through each symbol represents the width at half-maximum of the PL spectra. Although our calculated band gap for the three prototype shapes follows the same curve, to simplify matters, we show in Figure 5 only the results for the spherical quantum dots. A Coulomb energy representing attraction between the excited electron in the conduction band and the hole in valence band was added to our calculated band gap E_{gap} in order to compare with the PL data. The exciton energy for a sphere is (in atomic unit, hartrees for energy and bohr radius for d):[45]

$$E_x = E_{gap} - \frac{3.572}{\epsilon d} - 0.248 E_{Ry} \qquad (9)$$

The second term is the Coulomb term, and the third term is a correlation energy correction. ϵ is the dielectric constant and $E_{Ry} = \mu\epsilon^4/2\epsilon^2\hbar^2$, where μ is the effective mass of electron–hole pair. We used the bulk Si value $\epsilon = 11.91$ and $E_{Ry} = 8.18$ meV. The resulting calculated curve is shown in Figure 5. While it is not clear whether the bulk ϵ value is appropriate for small quantum dots,[46] the large experimental uncertainty prevents us from assessing the best value of ϵ. Given this large size distribution, we can only conclude that our calculated result agrees with the experimental data within the experimental uncertainty. This large experimental uncertainty also prevents us from determining at present which direct calculation results in Figure 4 agrees best

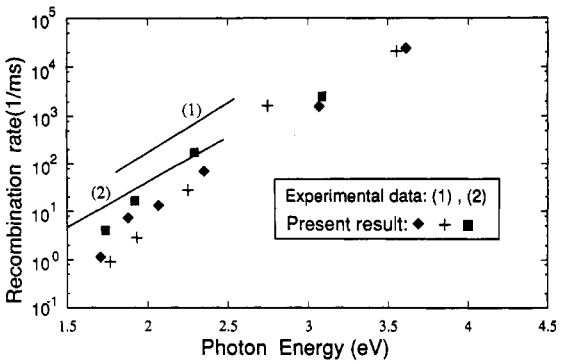

Figure 6. Radiative recombination rate $1/\tau$ (eq 10) as a function of the luminescence photon energy (excitonic band gap). Experimental curves 1 and 2 are from ref 7 and 47, respectively. The symbols ◆, +, and ■ represent calculations for spherical, (110) × (1$\bar{1}$0) × (001) rectangular, and (100) × (010) × (001) cubic quantum dots. The Coulomb interaction energy (eq 9) has been added to the calculated band gap.

with experiment. It would clearly be desirable to synthesis Si dots with a tighter size control.

F. Radiative Recombination Rate *vs* Quantum Dot's Size. Figure 6 depicts the calculated radiative recombination rate *vs* the band gap for our three prototype quantum dots. The results are compared with the experimental data.[7,47] The recombination rate is defined as $1/\tau$; here τ is the radiative lifetime, calculated from[48]

$$\frac{1}{\tau} = \frac{4}{3}\frac{\alpha\omega n}{m_e^2 c^2}\langle i|p|f\rangle^2 \qquad (10)$$

Here, n(=2.6) is the effective refractive index of Si quantum dot,[49] ω is the photon angular frequency, $\alpha = e^2/\hbar c$, and the matrix element $\langle i|p|f\rangle$ represents purely electronic wave functions, ignoring the contribution from atomic vibrations. The value of τ calculated from eq 10 strictly between the HOMO and LUMO states fluctuates widely even with small changes in quantum dot's size. To reduce this fluctuation, we have taken an average of $\langle i|p|f\rangle^2$ over the four highest occupied states i and four lowest unoccupied states f. The energy spread for these four eigenstates is about 20 meV for the largest quantum dots studied here, thus of the order of kT at room temperature. Figure 6 shows that, unlike the E_g *vs* d curves (Figure 2), which collapse into a single "unified" curve for all prototype quantum dots, the $1/\tau$ *vs* d curve shows some scatter and does not collapse into a universal curve for all quantum dot shapes. In the small band gap (large size) region, cubic quantum dots have a larger recombination rate, followed by spherical quantum dots, and then by rectangular quantum dots. Our results agree qualitatively with the experimental data[7,47] in that the difference between the experimental data and the current result is in the same order of magnitude as the difference between the two sets of the experimental data.

G. Orientation Dependence. We have next studied the effect of the surface orientation of the quantum dot on its band gap and recombination rate: To eliminate other effects, we have chosen two quantum dots with the same shape (cubic) and almost the same sizes (differing by 1.7%). One quantum dot has (100), (010), and (001) surfaces, and the other has (110), (1$\bar{1}$0), and (001) surfaces. Thus, the latter structure represents a 45° rotation of the first structure around one of its principal axes. The calculated band gaps and radiative lifetimes are given in Table 2. After correcting the small size difference using the unified curve of Figure 2, we find that the band gap difference for these two orientations is 0.014 eV. This is only 2% of the band gap blue shift (ΔE_g) and is thus negligible. However, the recombination rate of the [(110),(1$\bar{1}$0),(001)] oriented quantum dot is 40 times smaller than that of the [(100),(010),(001)] oriented quantum dot (similar to the situation in Figure 6). We can conclude that the band gap energy has negligibly small dependence on orientation, but the radiative lifetime (recombination rate) is more sensitive to it.

TABLE 2: Orientation Dependence of the Band Gap and Radiative Lifetime of Cubic Quantum Dots[a]

system	orientation	N_{Si}	N_H	d (Å)	E_{gap} (eV)	τ (μs)
1	(100) × (010) × (001)	1101	532	34.783	1.8173	231.2
2	(110) × (1$\bar{1}$0) × (001)	1157	492	35.363	1.8237	8647

[a] The band gap difference after correcting for the small difference in size is 0.014 eV.

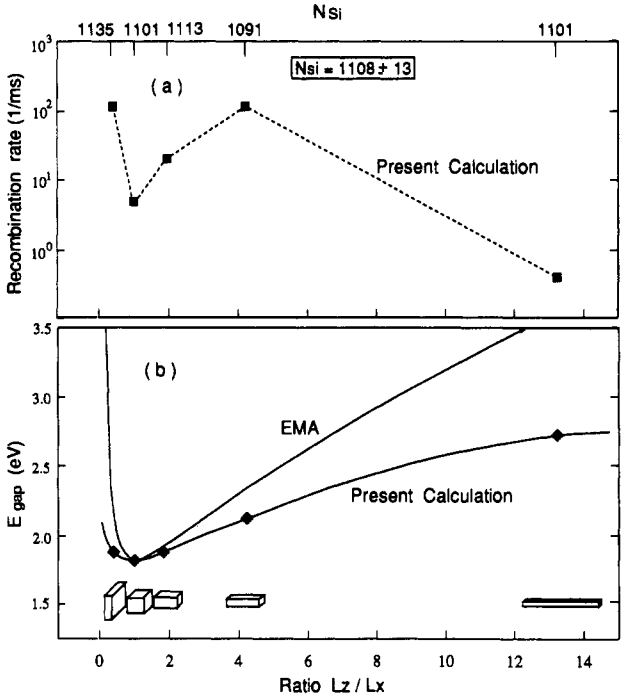

Figure 7. Dependence of the band gap and recombination rate ($1/\tau$) on the shape $L_z/L_x = L_z/L_y$ of Si quantum boxes. The box has the (100) × (010) × (001) orientation. The ratio L_z/L_x changes from 0.38 to 13.2, and the box changes from filmlike to wirelike. (a) The radiative recombination rate ($1/\tau$) *vs* ratio L_z/L_x. (b) The band gap *vs* the ratio L_z/L_x.

H. Shape Dependence at Constant Size. Quantum confinement effects can exist in one-dimension (film), two-dimension (wire), and three-dimension (particle) systems. In Figure 2, we showed that if the effective size is measured as $d \propto N_{Si}^{1/3}$, the band gap *vs* size (or N_{Si}) curves are similar for three prototype shapes, as long as the structure is not too prolate. It would be interesting to study the band gap change when a quantum dot goes through an extreme shape change, e.g., from a filmlike object to a wirelike object. We examined this by changing the aspect ratio $L_z/L_x = L_z/L_y$ of a rectangular box (see inserts to Figure 7): When the ratio $L_z/L_x \ll 1$, the quantum dot is filmlike; when $L_z/L_x = 1$, the quantum dot is cubic; and when $L_z/L_x \gg 1$, the quantum dot is wirelike. To eliminate the effects of orientation, we studied boxes with fixed surface orientations [(100),(010),(001)] for all L_z/L_x ratios. To eliminate the effect of size N_{Si}, we studied quantum dots having almost the same number $N_{Si} = 1108 \pm 13$ of Si atoms. Figure 7 depicts the recombination rate (part a) and band gap energy (part b) versus the ratio L_z/L_x. Note that different shapes at $N_{Si} \cong$ constant can have gaps that differ by as much as 0.8 eV. The structure with the smallest band gap (i.e., weakest quantum confinement effect) occurs when $L_z/L_x = 1$ (cubic). Fitting the $L_z/L_x = 1$ point to an EMA formula shows that when L_z/L_x differs from 1, the effective mass formula overestimates the quantum confinement effects. This is consistent with the results of Figure 2, which indicates that the smaller the length L_x or L_z, the larger the error of the EMA.

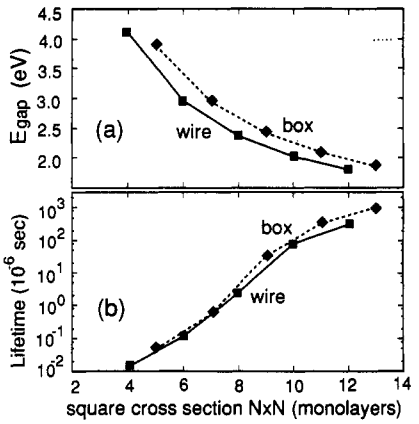

Figure 8. Comparison of the band gap and radiative lifetime (τ) of finite rectangular quantum boxes of length $L_z = \sqrt{2}L_x = \sqrt{2}L_y$ and infinitely long ($L_z = \infty$) quantum wires. In both cases, the cross section perpendicular to the z direction is $[(100),(1\bar{1}0)]$, and there are N Si monolayers on each sides. The distance between two Si monolayers is 1.92 Å. The quantum wire results are taken from ref 13b with adjustments (for the effective refractive index n and the way of averaging matrix element $\langle i|p|f\rangle^2$ in eq 10), so that the same way of calculating τ is used as described in section III.F.

An interesting point gleaned from Figure 7a concerns the recombination rate of the longest wirelike system ($L_z/L_x = 13.22$). Although the band gap of this wirelike system is larger than the gaps of other systems (indicating a stronger quantum confinement effect for the band gap), the recombination rate is smaller than the other systems (indicating a weaker quantum confinement effect as far as the rate is concerned). This can be understood as follows: The band gap increase is determined by the two smallest confining dimensions L_x and L_y; thus, the wirelike system shows a large band gap increase. However, we find from the projection analysis of the wave function that the k points of eq 8 have k_z components which equal roughly $k_z = \pi/L_z + 0.34\pi/a_0$ for the HOMO and $k_z = \pi/L_z$ for the LUMO (a_0 is the bulk lattice constant). According to the product of the HOMO and LUMO envelop functions, the matrix element $\langle i|p|f\rangle^2$ is roughly proportional to $(0.34\,(\pi/a_0)L_z)^{-2}$ and is thus small because of the large value of L_z. Extrapolating from this, one can conclude that in some infinitely long quantum wires the band gap could be very large due to quantum confinement, yet the recombination rate could still be small because of the nonzero k_z value of the HOMO state. The fact that HOMO and not LUMO has a nonzero k_z point in the wirelike system is interesting. It is the bulk Si conduction band minimum and not the valence band maximum which has a nonzero k_z point. This may be a result of an interplay between the quantum confinement effect and multiband coupling, because a single band model would not predict a nonzero k_z point for HOMO state. Notice that the first principle LDA calculations[50-52] of [001] oriented quantum wires do not give nonzero k_z HOMO states. However, the wire cross sections of these LDA calculations are squares with the $[(110),(1\bar{1}0)]$ orientations, while we have used square cross sections in the $[(100),(010)]$ orientation in our calculations. Also, from Figure 1 of ref 51, one can see that the k_z dispersion of the HOMO state is very flat (flatter than that of LUMO state). So it is easier to develop a nonzero k_z at the HOMO than at the LUMO state.

It is interesting to compare the band gap and radiative lifetime of rectangular boxs (finite L_z) to those of infinitely long ($L_z = \infty$) quantum wires. In both cases, we use structures with cross section $[(110),(1\bar{1}0)]$. The results of our rectangular box are given in Figures 2 and 6. The results of the quantum wire are from ref 13b. (The HOMO and LUMO for these quantum wires have $k_z = 0$.) The comparison in Figure 8 shows that (i) given the same $[(110),(1\bar{1}0)]$ cross sections for the wire and rectangular box, the box has a band gap 0.2–0.3 eV higher than that of the wire (in the cross section size range 10–20 Å) and (ii) the radiative lifetimes for these two systems are very close, within a factor of 2. The fact that the gap of a dots is larger than that of the wire is consistent with the larger quantum confinement for finite L_z (i.e., box). However, the nearly identical radiative lifetimes of these two systems is surprising given that in the wire $k_z = 0$ for the HOMO and LUMO while in the box $k_z \neq 0$ for both of them. This implies that, in this case, the radiative lifetime is mostly determined by the x, y directions, while the z direction has little effect.

IV. Conclusions

We have used the empirical pseudopotential method to calculate the electronic structure of Si quantum dots of different sizes, shapes, and orientations. This was made possible by a newly developed calculational method which enables one to calculate the eigenstates within a desired "energy window" in a linear-in-size scaling. Realistic surface relaxations are used, and the surface density of states are fitted to give the surface hydrogen potential. We found that:

(i) A unified band gap *vs* size curve exists for a few prototype quantum dot shapes.

(ii) The band gap is rather insensitive to the orientation and the shape as long as the shape is not too prolate.

(iii) In contrast, the radiative lifetime is more sensitive to the shape and orientation.

(iv) The HOMO and LUMO are bulklike states; thus, once the system is passivated, surface atoms have little direct effect to the band gap and radiative lifetime.

(v) The effective mass model *overestimates* the band gap blue shift mostly because of the assumed parabolic scaling. The latter approximation reflects the retention of kinetic energy and neglect of potential energy. The simple truncated crystal model *underestimates* the blue shift because of the neglect of band mixing.

(vi) Comparison to other direct calculation results reveals that the longer than nearest-neighbor interaction and the overlapping matrix of the basis are important in the tight-binding Hamiltonian in order to give the right band gap *vs* size relation.

Acknowledgment. We thank M. P. Teter for discussion on the convergence of the numerical scheme, S. Froyen for giving technical support with the computer system, and C. Y. Yeh and S. B. Zhang for many helpful discussions. This work was supported by the office of Energy Research, Materials Science Division, U.S. Department of Energy, under Grant DE-AC02-83CH10093.

References and Notes

(1) Bawendi, M. G.; Stiegerwald, M. L.; Brus, L. E. *Annu. Rev. Phys. Chem.* **1990**, *41*, 477. See also the June 1993 issue of *Phys. Today*.

(2) Reed, M. A. *Sci. Am.* **1993**, *268*, 118.

(3) Saunders, W. A.; Atwater, H. A.; Vahala, K. J.; Flagan, R. C.; Sercel, P. C. *Mater. Res. Soc. Symp.* **1993**, *283*, 77.

(4) Takagi, H.; Ogawa, H.; Yamazaki, Y.; Ishizaki, A.; Nakagiri, T. *Appl. Phys. Lett.* **1990**, *56*, 2379.

(5) Littau, K. A.; Szajowski, P. J.; Muller, A. J.; Kortan, A. R.; Brus, L. E. *J. Phys. Chem.* **1993**, *97*, 1224.

(6) Canham, L. T. *Appl. Phys. Lett.* **1990**, *57*, 1046.

(7) Xie, Y. H.; Wilson, W. L.; Ross, H. M.; Mucha, J. A.; Fitzgerald, E. A.; Macaulay, J. M.; Harris, T. D. *J. Appl. Phys.* **1992**, *71*, 2403.

(8) Hartree, D. R. *Calculation of Atomic Structure*; John Wiley and Sons: New York, 1957.

(9) Hohenberg, P.; Kohn, W. *Phys. Rev.* **1964**, *136B*, 864. Kohn, W.; Sham, L. J. *Phys. Rev.* **1965**, *140A*, 1133.

(10) See: Bastard, G. *Wave Mechanics Applied to Semiconductor Heterostructure*; Paris, 1990.

(11) Luttinger, J. M.; Kohn, W. *Phys. Rev.* **1955**, *97*, 869.

(12) Rama Krishna, M. V.; Friesner, R. A. *Phys. Rev. Lett.* **1991**, *67*, 629.

(13) (a) Applications to quantum films are given in: Zhang, S. B.; Yeh, C. Y.; Zunger, A. *Phys. Rev. B* **1993**, *48*, 11204. (b) Applications to quantum wires are given in: Yeh, C. Y.; Zhang, S. B.; Zunger, A. *Appl. Phys. Lett.* **1993**, *63*, 3455.

(14) See: Harrison, W. A. *Electronic Structure and Properties of Solids*; Freeman: San Francisco, 1980.

(15) Delley, B. *J. Chem. Phys.* **1991**, *94*, 7245.
(16) Cohen, M. L.; Chelikowsky, J. R. *Electronic Structure and Optical Properties of Semiconductors*; Springer-Verlag: Berlin, 1988.
(17) Payne, M. C.; Teter, M. P.; Allan, D. C.; Arias, T. A.; Joannopoulos, J. D. *Rev. Mod. Phys.* **1992**, *64*, 1045.
(18) Wang, L. W.; Zunger, A. *J. Chem. Phys.*, in press.
(19) Welkowsky, M.; Braunstein, R. *Phy. Rev. B* **1972**, *5*, 497.
(20) Spicer, W. E.; Enden, R. C. In *Proceedings of the Ninth International Conference of the Physics of Semiconductors*; Ryvkin, S. M., Ed.; Nauka: Moscow, 1968; Vol. 1, p 65.
(21) Hulthen, R.; Nilsson, N. G. *Solid State Commun.* **1976**, *18*, 1341.
(22) Bludau, W.; Onton, A.; Heinke, W. *J. Appl. Phys.* **1974**, 1846.
(23) Ley, L.; Kowalcyzk, S. P.; Pollak, R. A.; Shirley, D. A. *Phys. Rev. Lett.* **1972**, *29*, 1088.
(24) Hensel, J. C.; Hasegawa, H.; Nakayama, M. *Phys. Rev.* **1965**, *138*, A225.
(25) Dzesselhaus, G.; Kip, A. F.; Kittel, C. *Phys. Rev.* **1955**, *98*, 368.
(26) Allen, F. G. *J. Phys. Chem. Solids* **1959**, *8*, 119.
(27) Chelikowsky, J. R.; Cohen, M. L. *Phys. Rev. B* **1974**, *10*, 5095.
(28) Pandey, K. C. *Phys. Rev. B* **1976**, *14*, 1557.
(29) Sakurai, T.; Hagstrum, H. D. *Phys. Rev. B* **1975**, *12*, 5349.
(30) Sakurai, T.; Hagstrum, H. D. *J. Vac. Sci. Technol.* **1976**, *13*, 807.
(31) Maruno, S.; Iwasaki, H.; Horioka, K.; Li, S. T.; Nakamura, S. *Phys. Rev. B* **1983**, *27*, 4110.
(32) Boland, J. J. *Phys. Rev. Lett.* **1990**, *65*, 3325.
(33) Kaxiras, E.; Joannopouplos, J. D. *Phys. Rev. B* **1988**, *37*, 8842.
(34) Northrup, J. E. *Phys. Rev. B* **1991**, *44*, 1419.
(35) Due to the intrinsic LDA error in the band gap (see ref 44), the exact position of the antibonding surface state is not known. However, we know that the conduction band energies should be shifted up relative to the LDA results and that the magnitude of the shift should be proportional to the total charge density at the location of the eigenstate. Consequently, we estimate that the lower bound of the antibonding surface state at Γ is 1 eV above the bottom of conduction band at that k point. Similar conclusions apply to other k points.
(36) See: Press, W. H.; Flannery, B. P.; Teukolsky, S. A.; Vettering, W. T. *Numerical Recipes*; Cambridge University Press: New York, 1989.
(37) Nishida, A.; Nakagawa, K.; Kakibayashi, H.; Shimada, T. *Jpn. J. Appl. Phys.* **1992**, *31*, L1219. Cole, M. W.; Harvey, J. F.; Lux, R. A.; Eckart, D. W. *Appl. Phys. Lett.* **1992**, *60*, 2800.
(38) Gavrilenko, V. I.; Vogl, P.; Koch, F. *Mater. Res. Soc. Symp. Proc.* **1993**, *283*, 431.
(39) Takagahara, T.; Takeda, K. *Phys. Rev. B* **1992**, *46*, 15578.
(40) Ren, S. Y.; Dow, J. D. *Phys. Rev. B* **1992**, *45*, 6492.
(41) Proot, J. P.; Delerue, C.; Allan, G. *Appl. Phys. Lett.* **1992**, *61*, 1948.
(42) Delley, B.; Steigmeier, E. F. *Phys. Rev. B* **1993**, *47*, 1397.
(43) Hirao, M.; Udo, T.; Murayama, Y. *Mater. Res. Soc. Symp. Proc.* **1993**, *283*, 425.
(44) Hybertson, M. S.; Louie, S. G. *Phys. Rev. B* **1986**, *34*, 5390. Goodby, R. W.; Schulter, M.; Sham, L. J. *Phys. Rev. B* **1988**, *37*, 10159.
(45) Brus, L. E. *J. Phys. Chem.* **1986**, *90*, 2555.
(46) Tsu, R.; Ioriatti, L.; Harvey, J. F.; Shen, H.; Lux, R. A. *Mater. Res. Soc. Symp. Proc.* **1993**, *283*, 437.
(47) Bsiesy, B.; Gaspard, F.; Herino, R.; Ligeon, M.; Muller, F.; Romestain, R.; Vial, J. C. Unpublished results (excerpted from ref 33).
(48) See: Dexter, D. L. In *Solid State Physics*; Seitz, F., Turnbull, D., Eds.; Academic: New York, 1958; Vol. 6, p 360.
(49) Jackson, W. B.; Johnson, N. M. *Mater. Res. Soc. Symp. Proc.* **1985**, *46*, 545.
(50) Read, A. J.; Needs, R. J.; Nash, K. J.; Canham, L. T.; Calcott, P. D. J.; Qteish, A. *Phys. Rev. Lett.* **1992**, *69*, 1232.
(51) Buda, F.; Kohanoff, J.; Parrinello, M. *Phys. Rev. Lett.* **1992**, *69*, 1272.
(52) Ohno, T.; Shiraishi, K.; Ogawa, T. *Phys. Rev. Lett.* **1992**, *69*, 2400.